

Electronic Origin of Phase Stability in Mg–Zn–Y Alloys with a Long-Period Stacking Order

Takao Tsumuraya^{1,2*}, Hiroyoshi Momida³, and Tamio Oguchi⁴

¹Priority Organization for Innovation and Excellence, Kumamoto University, Kumamoto 860-8555, Japan

²Magnesium Research Center, Kumamoto University, Kumamoto 860-8555, Japan

³The Institute of Scientific and Industrial Research, Osaka University, Ibaraki 567-0047, Japan

⁴Center for Spintronics Research Network, Osaka University, Toyonaka 560-8531, Japan

The origin of the phase stability of 18R Mg–Zn–Y alloys with a long-period stacking order (LPSO) is studied using first-principles calculations. We calculate the heat of formation as a function of the number of Zn vacancies to discuss the role of Zn atoms. The calculated convex hull indicates that the Zn atoms in the LPSO alloys are stable even if they number about half of the Y atoms. The bonding state with Zn *p* orbitals leads to the stability of the LPSO structure because the partial density of states of Mg nearest to the solute cluster forms a valley structure.

Long-period stacking order (LPSO) is a unique crystal structure, where its stacking faults (i.e., Shockley partial dislocations) are ordered periodically along with the stacking direction of close-packed planes.^{1–3)} In the early 1950s, Suzuki proposed that when solute atoms enter a face-centered cubic (fcc) metal, the chemical potential of the solute element is different from that of the fcc metal matrix, resulting in segregation of the solute element from the stacking fault.^{4,5)} This phenomenon was observed in various alloy systems.^{6,7)}

In 2001, a dual phase magnesium (Mg) alloy with a nominal composition of Mg–1Zn–2Y (at.%) composed of a LPSO structured phase and an α -Mg phase was discovered to exhibit a tensile yield strength of more than 600MPa and an elongation to fracture of 5%.⁸⁾ Since then, attention has been focused on developing high-strength Mg-based alloys containing LPSO, which promotes kink strengthening mechanisms.^{9,10)}

The LPSO structure in the Mg–Zn–Y alloys exhibits both chemical and stacking order. As illustrated in Fig. 1(a), a concentration of solute atoms (Zn and Y) on the (0001) plane appears in a few layers of the hexagonal close-packed (hcp) Mg matrix.¹¹⁾ As proposed by Suzuki,⁴⁾ Shockley partial dislocations occur in the solute-enriched layers. In early studies, this alloy was considered to have a $6H_2$ structure with an ABCBCB' stacking sequence,

*E-mail: tsumu@kumamoto-u.ac.jp

where A and B' layers are enriched by Zn and Y.^{11,12)} Some later studies showed that the $6H_2$ structure was incorrect; it is actually the $18R$ structure.^{13,14)} Three other structural polytypes of $10H$, $14H$, and $24R$ were also identified using a scanning transmission electron microscope (STEM).^{14–18)} The STEM measurements also revealed that solute elements are enriched as chemically ordered $L1_2$ -type Zn_6Y_8 clusters in the Mg matrix.¹⁶⁾ The presence of the $L1_2$ clusters causes anisotropic plastic deformation in Mg–Zn–Y alloys. The LPSO structure might prevent dislocations from moving across the cluster-arranged layer, namely, non-basal slips and deformation twins, and limit the movement only along the direction parallel to the close-packed plane (basal plane).^{9,10,19)} However, it is unclear what role the chemical bonds involving solute elements play in the mobility of dislocations. Furthermore, several experiments have reported various chemical compositions of Zn and Y for the LPSO structure,²⁰⁾ such as Mg–2Zn–4Y,¹¹⁾ Mg–3Zn–10Y,¹²⁾ Mg–4Zn–8Y,²¹⁾ Mg–2Zn–8Y,²²⁾ and Mg–6Zn–9Y alloys¹⁶⁾ (at. %).

However, the arrangement of Zn and Y in the diverging compositions remains unclear due to the difficulty of the experimental characterization of structural properties. Some previous works with first-principles calculations have been performed for fully crystalline LPSO alloys,^{23–27)} without considering the effect of vacancies. More recently, Y atoms were found to play a role in reducing energy barriers to forming a stacking fault,²⁸⁾ but the role of Zn atoms has not been clarified.

This study aims to understand the electronic origin of the phase stability of Mg–Zn–Y alloys containing LPSO using first-principles calculations based on density functional theory (DFT). In particular, we focus on the role of Zn in LPSO alloys and discuss the effects of the formation of Zn vacancies.

Generally, the density of states (DOS) of metals with an hcp structure is characterized by a deep valley around the Fermi energy (E_F).^{29–31)} The depth of the valley in DOS represents the magnitude of splitting of the peaks in the occupied and unoccupied states,²⁹⁾ which is an energy separation between the bonding and antibonding orbitals.³²⁾ Furthermore, by comparing electronic states between hcp Mg and hcp Be, Inoue and Yamashita suggested that the degree of energy splitting between the two peaks (the width of the deep valley or dip) appears as a difference in the enthalpy of formation between the metals.^{29,30)} Mackintosh and Andersen derived the force theorem:³³⁾ the change in the total energy of an electron system can be calculated as the difference of appropriate sums of the eigenvalue.^{34,35)} Therefore, the phase stability analysis based on DOS near Fermi energy may be understood by the energy change based on the force theorem.³⁶⁾

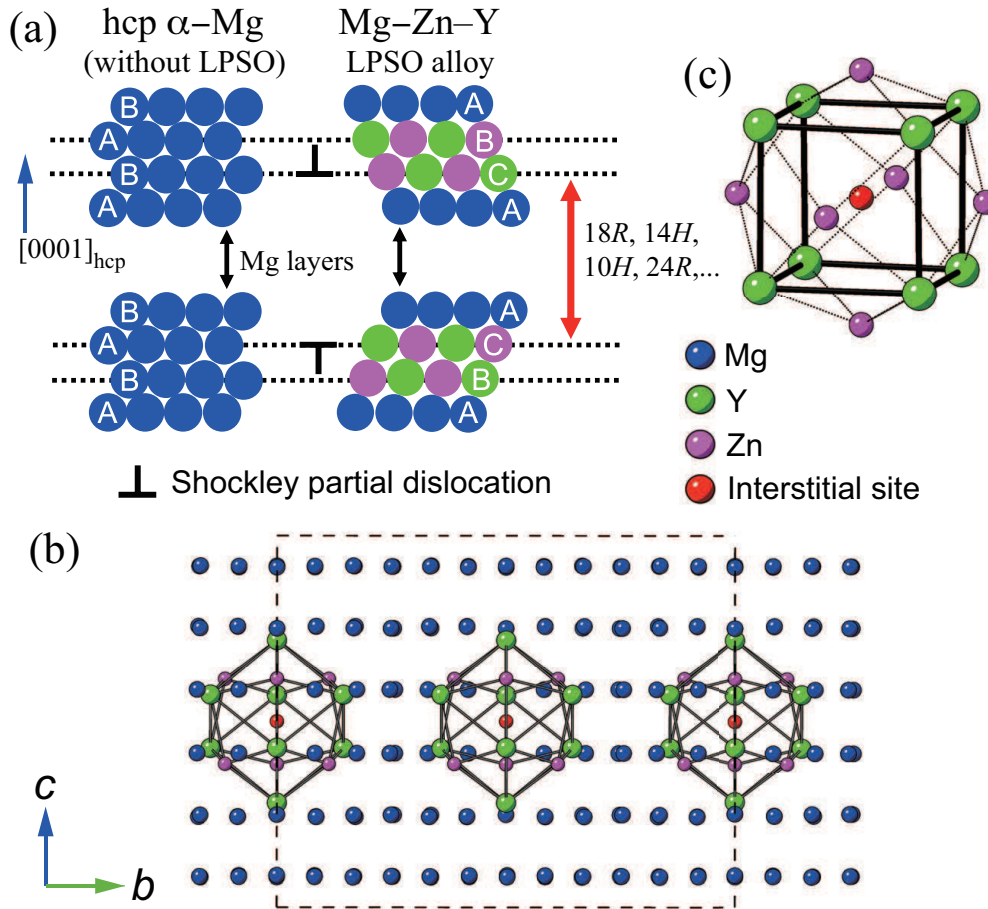


Fig. 1. (Color online) (a) Schematic diagrams of the hcp α -Mg and LPSO structure in Mg-Zn-Y alloy. (b) LPSO structure of $\text{Mg}_{58}\text{Zn}_6\text{Y}_8$ with an interstitial atom (monoclinic structure with the $C2/m$ space group). The unit cell is depicted with the dashed line. (c) Isolated Zn_6Y_8 $L1_2$ -arranged cluster, where the Zn atoms move away from a plane formed by four Y atoms (bold lines). The cluster is rotated from (b) to clearly display the $L1_2$ -arrangement of Zn and Y atoms.

The 18R LPSO structure is often observed in the Mg-Zn-Y system³⁷⁾ and thus the present calculations are based on an 18R structure with a base-centered monoclinic structure (space group: $C2/m$), determined by STEM measurements.^{15,16,38)} The 18R crystal structure observed after heat treatment at 500°C for 300 hours has another type of monoclinic cell (space group: $C2/c$).²⁶⁾ The latter structure has twice as many atoms as the former. However, we use the former structure in this study because there is little difference in the formation energy²⁶⁾ and electronic states between these two structures.

The observed solute atoms cluster embedded in the Mg matrix is distorted from the ideal $L1_2$ structure as illustrated in Fig. 1(b), where Zn atoms move away from the plane formed by four Y atoms [Fig. 1(c)]. Previous DFT studies have verified the distortion of the

cluster through structural optimization, which creates a sizable interstitial site at the body center of the $L1_2$ cluster.³⁹⁾ The inclusion of an atom at the central site stabilizes the LPSO structure.^{23–26,39,40)} The calculations verified that heat of formation is gained by about 20 to 24 meV compared to the absence of an interstitial atom.⁴¹⁾ To discuss the stability of Zn vacancies along a line in the ternary Mg–Zn–Y phase diagram (Zn composition ratio), we use the case of Zn as the central element.⁴¹⁾

In the present calculations, one-electron Kohn–Sham equations are solved self-consistently using a pseudopotential technique with plane wave basis sets adopting the projected augmented-wave method⁴²⁾ implemented in QUANTUM ESPRESSO.⁴³⁾ The exchange–correlation functional is the generalized gradient approximation proposed by Perdew, Burke, and Ernzerhof.⁴⁴⁾ The pseudopotentials in PSLibrary were used⁴⁵⁾ and were generated using atomic code (version 6.3) with a pseudization algorithm proposed by Troullier and Martins.⁴⁶⁾ The cutoff energies for plane waves and potential were set at 90 and 588 Ry, respectively. The dimensions of the \mathbf{k} -point mesh for the 18R LPSO structure are $6 \times 6 \times 4$ using the Gaussian smearing method during self-consistent loops, where the width of the smearing function is 0.02 Ry. The convergence threshold is 10^{-8} Ry. The DOS calculations use the \mathbf{k} -point dimensions of $8 \times 8 \times 4$ with the improved tetrahedron method.⁴⁷⁾

We first discuss the thermodynamic stability of the Zn vacancy by calculating the heat of formation as a function of the number of Zn vacancies (x). Figure 2(a) presents a magnified section of the ternary Mg–Zn–Y phase diagram. The red filled circle in the phase diagram indicates the number of atoms in the primitive cell of the $C2/m$ (18R) structure with the interstitial atom of Zn, $\text{Mg}_{58}\text{Zn}_7\text{Y}_8$, and thus the total number of atoms is 73. The asterisks on the bold line indicate each structure of 18R- $\text{Mg}_{58}\text{Zn}_{7-x}\text{Y}_8$, including Zn vacancies from $x = 0$ to 6, that is, the number of Zn atoms in $\text{Mg}_{58}\text{Zn}_{7-x}\text{Y}_8$ is deduced using the fixed number of Mg and Y atoms.

To understand whether the Mg–Zn–Y alloy, including Zn vacancies, can be formed from the elemental metals of Mg, Zn, and Y, the heat of formation for a specific Zn vacancy number, x , is defined as

$$\Delta H_f(x) = \frac{1}{(73 - x)} [E(\text{Mg}_{58}\text{Zn}_{7-x}\text{Y}_8) - 58E(\text{Mg}) + (7 - x)E(\text{Zn}) + 8E(\text{Y})], \quad (1)$$

where $E(\text{Mg}_{58}\text{Zn}_{7-x}\text{Y}_8)$ is the total equilibrium energy of the 18R-LPSO alloy with vacancy (x). For each vacancy state, we deduced all the possibilities of extracting x atoms from the

seven Zn sites in the Mg–Zn–Y alloy system. Subsequently, the lattice parameters and internal coordinates were optimized. The lattice parameters for $x = 0$ are $a = 11.1$, $b = 19.3$, $c = 16.1$ Å, and $\beta = 76.6^\circ$, which agree well with experiments [$a = 11.1$, $b = 19.4$, $c = 15.6 (= 46.89/3)$ Å, and $\beta = 83.3^\circ$].^{15,37)}

In Figs. 2(b) and 2(c), we plot only the energy values for the most stable structure. $E(M)$ denotes the equilibrium energy per atom of the elemental metals and is used as a reference of the chemical potential. Details are presented in the Supplementary Material.⁴¹⁾

Figure 2(b) displays the scatter plot of the heat of formation, ΔH_f , as a function of the Zn composition ratio, calculated with Eq. (1). The Zn composition ratio (at%) is calculated according to $(7-x)/(73-x) \times 100\%$, which corresponds to the bold line in Fig. 2(a). If the composition of Zn is zero ($x = 7$), it is a pseudo compound of Mg_{58}Y_8 . The ΔH_f of Mg_{58}Y_8 calculated from the LPSO structure is unstable compared to the sum of the total energy of the elemental metals of hcp Mg and hcp Y. Thus, in Fig. 2(b), the energy references are set at the sum of the total energy of the elemental metals, $58E(\text{Mg}) + 8E(\text{Y}) + (7-x)E(\text{Zn})$. Figure 2(b) suggests that all phases, including Zn vacancies ($x = 1 \sim 6$), are slightly above the bold line connecting $x = 0$ and $x = 7$. Therefore, these phases are thermodynamically unstable and decompose into $\text{Mg}_{58}\text{Zn}_7\text{Y}_8$ ($x = 0$) and elemental $58\text{Mg}+8\text{Y}$ ($x = 7$). Nevertheless, this diagram indicates that the distance from the hull decreases as the number of vacancies (x) decreases, where the energy differences between the red circles and the line connecting ΔH_f of $x = 0$ and $x = 7$ are closer.

Next, we consider the state in which Zn_7Y_8 clusters with an $L1_2$ structure are already formed in the Mg matrix and examine the convex hull when the ratio of Mg and Y is constant and only the atomic weight of Zn changes. For the convex hull, the formation energy as a function of x is calculated as

$$\Delta E(x) = E(\text{Mg}_{58}\text{Zn}_{7-x}\text{Y}_8) - \left\{ \frac{(6-x)}{6} E(\text{Mg}_{58}\text{Zn}_7\text{Y}_8) + \frac{x}{6} E(\text{Mg}_{58}\text{ZnY}_8) \right\}. \quad (2)$$

As plotted in Fig. 2(c), the energies of $x = 1$ and 3 lie on the convex hull. Therefore, incomplete $L1_2$ clusters with $x = 1$ and 3 are stable, suggesting that this can be observed below the decomposition temperature. Especially, at $x = 3$, the energy is the lowest in the convex hull and such an LPSO structure with a concentration ratio of Zn: Y = 1:2 is abundantly observed.^{8,11,13,21)}

On the contrary, the energy at $x = 2$ is slightly above the line connecting $x = 1$ and $x = 3$, and the system decomposes into $x = 1$ and $x = 3$. However, $x = 2$ is metastable since the

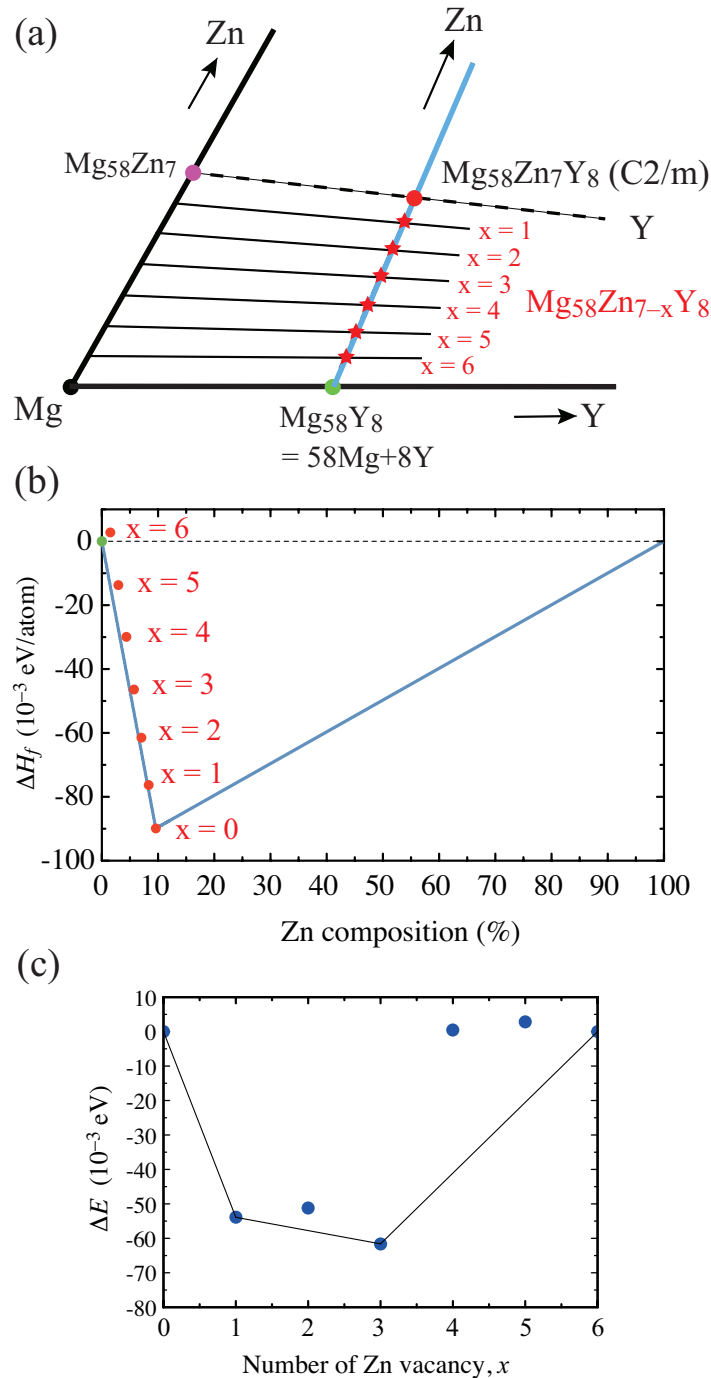


Fig. 2. (Color online) (a) Magnified section of ternary Mg–Zn–Y phase diagram. The red symbol on the diagram marks the constitution of $Mg_{58}Zn_7Y_8$, which indicates the number of atoms in the primitive unit cell of the 18R structure. The red asterisk indicates the 18R structure, including Zn vacancies, of $Mg_{58}Zn_{7-x}Y_8$, in which the number of Zn vacancies (x) is changed. $Mg_{58}Y_8$ and $Mg_{58}Zn_7$ are pseudo compounds. (b) Scatter plot of $\Delta H_f(x)$ calculated based on Eq. (1). The horizontal axis represents the Zn composition ratio $(7-x)/(73-x)$. We set the zero energy on the vertical axis at $58E(Mg) + 8E(Y) + (7-x)E(Zn)$ as the reference. (c) Convex hull for the number of Zn vacancies (x) in $Mg_{58}Zn_{7-x}Y_8$ alloy, with reference energies set at $x = 0$ and $x = 6$. The formation energy is calculated based on Eq. (2).

energy difference between the energy at $x = 2$ and the line connecting $x = 1$ and 3 is relatively small. In addition, the energies at $x = 4, 5,$ and 6 are unstable. Therefore, the Zn atoms in the LPSO alloy are stable even if they are approximately half of the number of Y atoms.

The convex hull plotted in Fig. 2(c) is obtained with the reference energy values at $x = 0$ and $x = 6$. However, the shape of the convex hull may change depending on the reference energies. The cases in which the reference energy is set at $x = 0$ and $x = 4$, and $x = 0$ and $x = 5$ are calculated and provided in the Supplementary Materials.⁴¹⁾ We came to the same conclusion as we did with $x = 0$ and $x = 6$ as the references.

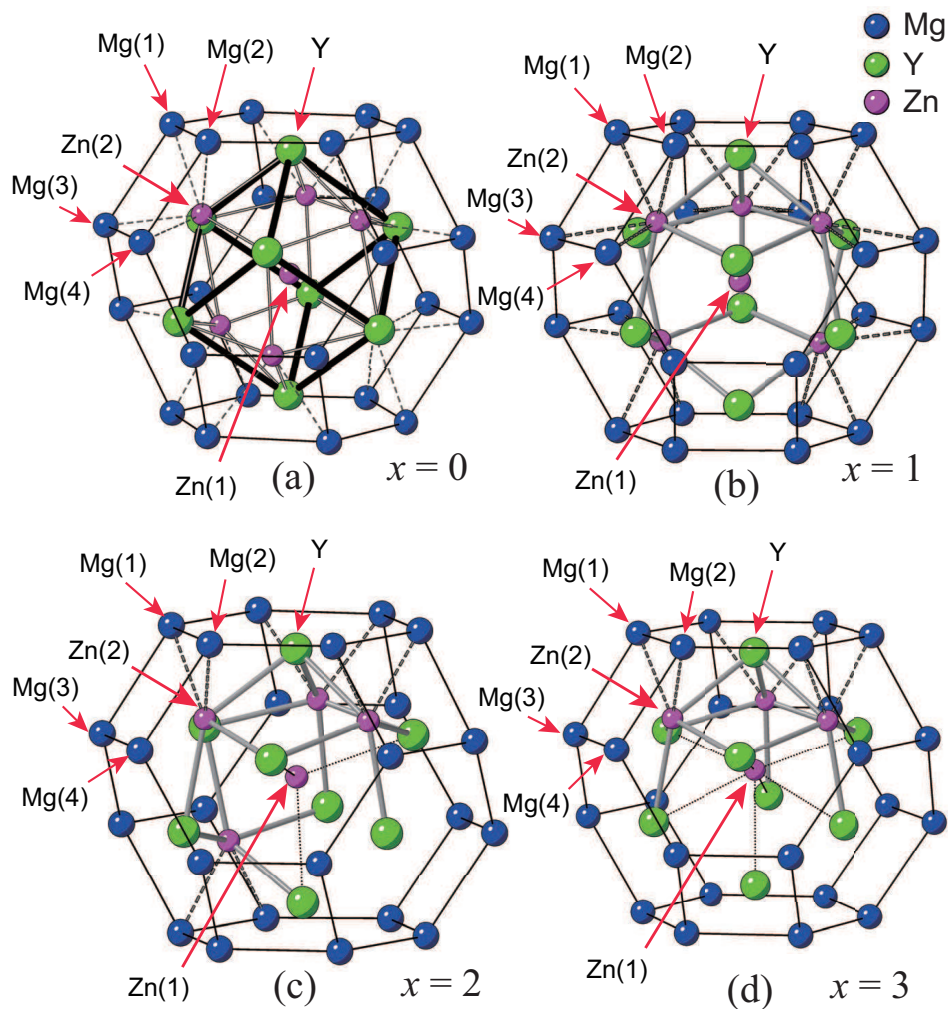


Fig. 3. (Color online) Geometry of the solute atom cluster and surrounding Mg atoms in $18R$ $Mg_{58}Zn_{7-x}Y_8$ alloy, where the number of Zn vacancies are (a) $x = 0$, (b) $x = 1$, (c) $x = 2$, and (d) $x = 3$. The most stable structure of each x is presented.

Finally, we examine the structural and electronic properties to elucidate the mechanism of stabilizing the Zn-vacancy-containing state. Figure 3 depicts the cluster of solute atoms

and surrounding Mg atoms in the most stable structures of each x . As depicted in Fig. 3(a), the interstitial atom of Zn is called Zn(1), and a Zn atom that forms the $L1_2$ cluster is called Zn(2). Two pyramids share the Zn atoms forming Mg_6Y_8 cage: one square pyramid is formed with the square planar of Mg, and the other is included with Y. The four Mg atoms nearest to the Zn atom are referred to as Mg(1) – Mg(4). In particular, the nearest-neighbor bonds to the Zn(2) atom are Mg atoms instead of Y atoms.

Observing the distances between these four Mg atoms and the Zn atom in Fig. 3, at $x = 1$, the length between Zn(2) and Mg(2) decreased by 0.01 \AA from that at $x = 0$, due to the formation of the Zn vacancy.⁴¹⁾ At $x = 3$, the distances from Zn(2) to both Mg(1) and Mg(2) decreased to 2.75 \AA , compared to 2.78 \AA at $x = 0$. These reductions in bond length indicate the strengthening of the bond between Mg and Zn. However, the distances to Mg(3) and Mg(4) from Zn(2) do not change much.⁴¹⁾ Therefore, in Fig. 4, we only present the projected DOS on p orbitals of Mg(1), Mg(2), Zn(1), Zn(2), and d orbitals of Y in $Mg_{58}Zn_{7-x}Y_8$ alloy with $x = 0, 1, 2,$ and 3 .

As mentioned earlier, the DOS of hcp metal has a valley and E_F is located near the lowest position of the valley. The width of the valley appears as a difference in heat of formation between the metals. The $18R$ Mg–Zn–Y alloy also has a DOS valley.²⁷⁾ However, the lowest DOS position is approximately 0.2 eV higher than E_F ,^{27,41)} as depicted in Fig. 4(a). Therefore, its more energetically favorable phase could form by introducing electron deficiencies.

We first examined the dependence of x on the total DOS.⁴¹⁾ It is discovered that the change in the DOS valley near E_F was not distinct compared to simple metals with LPSO structure in Fe.³⁶⁾ Thus, we used the projected DOS of Zn and its neighboring Mg and plotted them in Fig. 4. As shown by the asterisks and triangles in Figs. 4(b) and 4(d), the presence of Zn vacancies causes DOS peaks of p states in Zn(2), Mg(1), and Mg(2) atoms around -0.8 eV . These Mg and Zn atoms form a bonding state below E_F , which reduces these partial DOS at E_F , and the width of the DOS valley of the Mg- p states increases compared to the case without vacancies in Fig. 4(a).

The p states of the Zn atoms also hybridize with the d orbitals of the neighboring Y atoms, as seen in the DOS dip above the E_F in Fig. 4(a). The d bands are partially filled with the d^1 configuration to form covalent bonds. The energy position (band filling) of the Y d state is hardly changed when Zn vacancies are introduced [Figs. 4(b)–4(d)]. Therefore, Zn atoms in the LPSO alloy could be responsible for adhering Y atoms to the surrounding Mg atoms.

Furthermore, as x increases, the partial DOS of Zn(1) at the interstitial sites becomes larger. Especially at $x = 3$, the p states of Zn(1) hybridize with those of Zn(2), and the

surrounding Mg atoms to form the bonding state below E_F , as shown in the peaks marked with asterisks in Fig. 4(d).

In conclusion, the convex hull we obtained at $x = 1$ and 3, below the decomposition temperature, suggests that the Zn atoms in the LPSO alloy are stable even if they number about half of the Y atoms. Focusing on the partial DOS of Zn and its neighboring Mg (the boundary between the solute cluster and the Mg matrix), we reveal that the partial DOS of Mg atoms at the interface forms a valley structure due to the bonding state with Zn atoms. The formation of the bonding state between Zn and the surrounding Mg atoms plays a crucial role in stabilizing the LPSO structure.

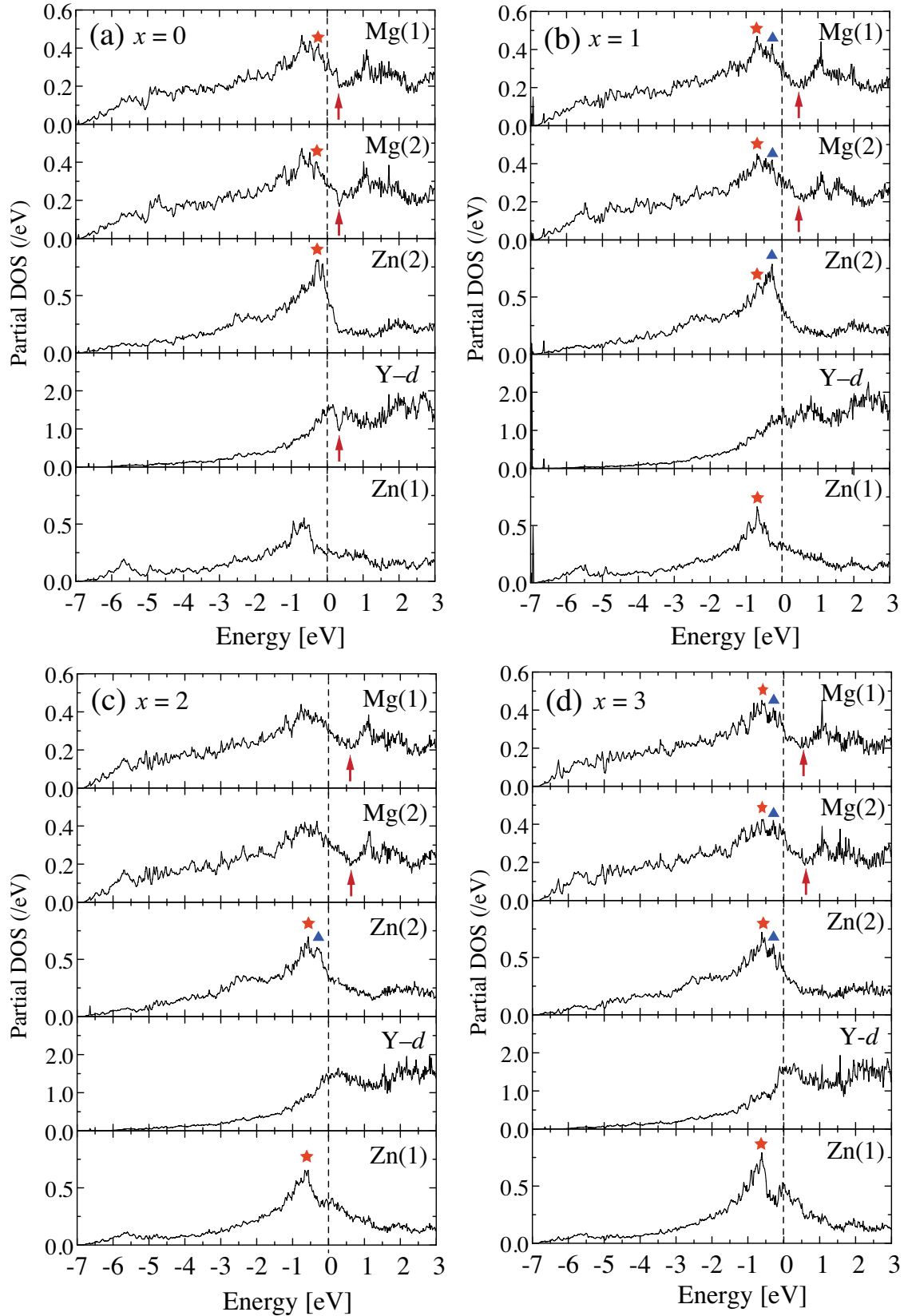


Fig. 4. Partial density of states (DOS) projected on the p orbitals of Mg, Zn, and d orbitals of Y in $18R\text{-Mg}_{58}\text{Zn}_{7-x}\text{Y}_8$ alloy, where (a) $x = 0$ (no vacancy), (b) $x = 1$, (c) $x = 2$, and (d) $x = 3$. The zero-energy with a longitudinal dashed line is the Fermi energy (E_F). Up arrows represent the bottom of the DOS dip.

References

- 1) H. Sato and R. S. Toth: Phys. Rev. **124** (1961) 1833.
- 2) L. I. Lysak and B. I. Nikolin: Dokl. Akad. Nauk SSSR **153** (1963) 812.
- 3) M. Oka, Y. Tanaka, and K. Shimizu: Jpn. J. of Appl. Phys. **11** (1972) 1073.
- 4) H. Suzuki: Sci. Rep. Res. Inst. Tohoku Univ. A **4** (1952) 455.
- 5) H. Suzuki: J. Phys. Soc. Jpn **17** (1962) 322.
- 6) T. Kamino, Y. Ueki, H. Hamajima, K. Sasaki, K. Kuroda, and H. Saka: Philos. Mag. Lett. **66** (1992) 27.
- 7) G. Han, I. Jones, and R. Smallman: Acta Mater. **51** (2003) 2731.
- 8) Y. Kawamura, K. Hayashi, A. Inoue, and T. Masumoto: Mater. Trans. **42** (2001) 1172.
- 9) K. Hagihara, N. Yokotani, and Y. Umakoshi: Intermetallics **18** (2010) 267.
- 10) X. Shao, Z. Yang, and X. Ma: Acta Mater. **58** (2010) 4760.
- 11) E. Abe, Y. Kawamura, K. Hayashi, and A. Inoue: Acta Metall. **50** (2002) 3845.
- 12) D. Ping, K. Hono, Y. Kawamura, and A. Inoue: Philos. Mag. Lett. **82** (2002) 543.
- 13) T. Itoi, T. Seimiya, Y. Kawamura, and M. Hirohashi: Scripta Mater. **51** (2004) 107.
- 14) M. Matsuda, S. Ii, Y. Kawamura, Y. Ikuhara, and M. Nishida: Mater. Sci. Eng. A **393** (2005) 269.
- 15) Y. Zhu, A. Morton, and J. Nie: Acta Mater. **58** (2010) 2936.
- 16) D. Egusa and E. Abe: Acta Mater. **60** (2012) 166.
- 17) M. Yamasaki, M. Matsushita, K. Hagihara, H. Izuno, E. Abe, and Y. Kawamura: Scripta Mater. **78** (2014) 13.
- 18) T. Kiguchi, Y. Ninomiya, K. Shimmi, K. Sato, and T. J. Konno: Mater. Trans. **54** (2013) 668.
- 19) J.-K. Kim, S. Sandlöbes, and D. Raabe: Acta Mater. **82** (2015) 414.
- 20) D. Drozdenko, M. Yamasaki, K. Máthis, P. Dobroň, P. Lukáč, N. Kizu, S. Inoue, and Y. Kawamura: Mater. Des. **181** (2019) 107984.
- 21) Y. Chino, M. Mabuchi, S. Hagiwara, H. Iwasaki, A. Yamamoto, and H. Tsubakino: Scr Mater **51** (2004) 711.
- 22) Y. M. Zhu, M. Weyland, A. Morton, K. Oh-ishi, K. Hono, and J. Nie: Scripta Mater. **60** (2009) 980.
- 23) J. E. Saal and C. Wolverton: Scripta Mater. **67** (2012) 798.
- 24) S.-Y. Ma, L.-M. Liu, and S.-Q. Wang: J. Mater. Sci. **48** (2013) 1407.
- 25) J. E. Saal and C. Wolverton: Acta Mater. **68** (2014) 325.

- 26) K. Kishida, K. Nagai, A. Matsumoto, A. Yasuhara, and H. Inui: *Acta Mater.* **99** (2015) 228.
- 27) Z.-N. Ma, X. Wang, T.-T. Yan, Q. Li, Q.-C. Xu, J.-L. Tian, and L. Wang: *J. Alloys. Comp.* **708** (2017) 29.
- 28) S. Kawano, S. Iikubo, and H. Ohtani: *Comp. Mater. Sci.* **171** (2020) 109210.
- 29) S. Inoue and J. Yamashita: *J. Phys. Soc. Jpn* **35** (1973) 677.
- 30) J. Yamashita: Kotai-densiron (in Japanese) (Asakura Publishing Co., Ltd., 1973).
- 31) A. T. Paxton, M. Methfessel, and D. G. Pettifor: *Proc. R. Soc. Lond. A* **453** (1997) 1493.
- 32) J. C. Slater: Quantum Theory of Molecules and Solids II (McGraw-Hill, 1965).
- 33) A. R. Mackintosh and O. K. Andersen: in Electrons at the Fermi surface, ed. M. Springford (Cambridge University Press, 1979).
- 34) V. Heine: *Solid State Phys.* **35** (1980) 1.
- 35) H. L. Skriver: *Phys. Rev. Lett.* **49** (1982) 1768.
- 36) T. Tsumuraya, I. Watanabe, and T. Sawaguchi: *Phys. Rev. Research* **3** (2021) 033215.
- 37) Y. Zhu, A. Morton, and J. Nie: *Acta Mater.* **60** (2012) 6562.
- 38) H. Yokobayashi, K. Kishida, H. Inui, M. Yamasaki, and Y. Kawamura: *Acta Mater.* **59** (2011) 7287.
- 39) D. Egusa, M. Mihalcovic, and E. Abe: Presented at International Symposium on Long-Period Stacking Ordered Structure and Its Related Materials 2012 at Sapporo, October 1-3, 2012.
- 40) M. Itakura, M. Yamaguchi, D. Egusa, and E. Abe: *Acta Mater.* **203** (2021) 116491.
- 41) see Supplementary Material.
- 42) P. E. Blöchl: *Phys. Rev. B* **50** (1994) 17953.
- 43) P. Giannozzi, O. Andreussi, T. Brumme, O. Bunau, M. B. Nardelli, M. Calandra, R. Car, C. Cavazzoni, D. Ceresoli, M. Cococcioni, N. Colonna, I. Carnimeo, A. D. Corso, S. de Gironcoli, P. Delugas, R. A. DiStasio, A. Ferretti, A. Floris, G. Fratesi, G. Fugallo, R. Gebauer, U. Gerstmann, F. Giustino, T. Gorni, J. Jia, M. Kawamura, H.-Y. Ko, A. Kokalj, E. Küçükbenli, M. Lazzeri, M. Marsili, N. Marzari, F. Mauri, N. L. Nguyen, H.-V. Nguyen, A. O. de-la Roza, L. Paulatto, S. Poncé, D. Rocca, R. Sabatini, B. Santra, M. Schlipf, A. P. Seitsonen, A. Smogunov, I. Timrov, T. Thonhauser, P. Umari, N. Vast, X. Wu, and S. Baroni: *J. Phys. Cond. Matter* **29** (2017) 465901.
- 44) J. P. Perdew, K. Burke, and M. Ernzerhof: *Phys. Rev. Lett.* **77** (1996) 3865.
- 45) A. Dal Corso: *Comp. Mater. Sci.* **95** (2014) 337.
- 46) N. Troullier and J. Martins: *Solid State Comm.* **74** (1990) 613.

47) M. Kawamura, Y. Gohda, and S. Tsuneyuki: Phys. Rev. B **89** (2014) 094515.

Acknowledgments

The authors thank Y. Kawamura, S. Ando, D. Shih, and M. Yamasaki for stimulating the discussion. This work was supported by the Cooperative Research Program of the Network Joint Research Center for Materials and Devices. This research was supported by a Grant-in-Aid for Scientific Research (Grants Nos. JP19K04988, JP20H00312, and JP22K04671) from the Japan Society for the Promotion of Science (JSPS) and a SICORP Grant (No. JPMJSC2109) and a CREST Grant (No. JPMJCR2094) from Japan Science and Technology Agency (JST). The calculations were conducted primarily at the Research Institute for Information Technology Computer Facilities at Kyushu University and MASAMUNE at the Institute for Materials Research, Tohoku University, Japan.

Supplementary Material for “Electronic Origin of Phase Stability in Mg–Zn–Y Alloys with Long-Period Stacking Order”

Takao Tsumuraya^{1,2}, Hiroyoshi Momida³, and Tamio Oguchi⁴

¹Priority Organization for Innovation and Excellence, Kumamoto University, Kumamoto 860-8555, Japan

²Magnesium Research Center, Kumamoto University, Kumamoto 860-8555, Japan

³The Institute of Scientific and Industrial Research, Osaka University, Ibaraki 567-0047, Japan

⁴Center for Spintronics Research Network, Osaka University, Toyonaka 560-8531, Japan

1. Effect of interstitial atoms on the electronic structure near the Fermi level

We show how the interstitial atom in the $Zn_6Y_8 L1_2$ cluster affects the heat of formation and the total density of states (DOS) around the Fermi energy (E_F). Egusa *et al.* originally reported that introducing an atom at the center of the Zn_6Y_8 cluster stabilizes the LPSO structure.¹⁾ For the 18R LPSO structure, we verified that the calculated heat of formation increased by approximately 20–25 meV/atom compared to that without an interstitial atom. The heat of formation for the 18R Mg-Zn-Y alloys is calculated as

$$\begin{aligned}\Delta H &= \{E(\text{Mg}_{58}\text{Zn}_6\text{Y}_8) - [58E(\text{Mg}) + 6E(\text{Zn}) + 8E(\text{Y})]\} / 72 \\ &= -70 \text{ meV/atom.}\end{aligned}\quad (\text{S1})$$

where 72 is the number of atoms in the primitive cell of the $C2/m$ structure without an interstitial atom. $E(\text{Mg})$, $E(\text{Zn})$, and $E(\text{Y})$ are the equilibrium total energy of the elemental metals.

With an interstitial atom, the total number of atoms is 73, and the heat of formation is calculated as

$$\begin{aligned}\Delta H_{int}^{\text{Mg}} &= \{E(\text{Mg}_{59}\text{Zn}_6\text{Y}_8) - [59E(\text{Mg}) + 6E(\text{Zn}) + 8E(\text{Y})]\} / 73 \\ &= -95 \text{ meV/atom}\end{aligned}\quad (\text{S2})$$

$$\Delta H_{int}^{\text{Zn}} = \{E(\text{Mg}_{58}\text{Zn}_7\text{Y}_8) - [58E(\text{Mg}) + 7E(\text{Zn}) + 8E(\text{Y})]\} / 73 \quad (\text{S3})$$

$$= -90 \text{ meV/atom.}$$

$$\begin{aligned} \Delta H_{int}^Y &= \{E(\text{Mg}_{59}\text{Zn}_6\text{Y}_9) - [58E(\text{Mg}) + 6E(\text{Zn}) + 9E(\text{Y})]\} / 73 \quad (\text{S4}) \\ &= -94 \text{ meV/atom} \end{aligned}$$

The order of stability is Mg, Y, and Zn for the types of interstitial atoms. From Table S1, these results generally agree with those from previous studies.²⁻⁵⁾ The calculated heat of formation with a Zn interstitial atom (-90 meV/atom) is higher than that with Mg and Y atoms of -95 meV/atom and -94 meV/atom , respectively. However, Zn and Y have been experimentally reported to be in the central position of the cluster.⁴⁾

Table S1. Calculated heats of formation ΔH_f for 18R LPSO structure with different types of interstitial atoms.

Interstitials	Formula	ΔH_f (meV/atom)	Previous studies
No atom	$\text{Mg}_{58}\text{Zn}_6\text{Y}_8$	-70	-70 ²⁾
Mg	$\text{Mg}_{59}\text{Zn}_6\text{Y}_8$	-95	-98 ³⁾
Y	$\text{Mg}_{58}\text{Zn}_6\text{Y}_9$	-94	
Zn	$\text{Mg}_{58}\text{Zn}_7\text{Y}_8$	-90	

We show that an increase in the heat of formation by adding an interstitial atom is related to the total DOS near the Fermi energy E_F . As described in the main text, the DOS of the metal with a hexagonal close-packed (hcp) structure is generally characterized by the presence of a deep valley or dip near E_F , where E_F is located at the lowest position of the DOS valley.⁶⁻⁹⁾ The depth of a DOS valley represents the magnitude of the splitting of the main DOS peaks between those in occupied and unoccupied states. The width of a valley or dip near E_F appears as a difference in the heat of formation (or cohesive energy) between different types of hcp metals.^{7,8)}

Figure S1(a) plots the total DOS of the 18R-type $\text{Mg}_{58}\text{Zn}_6\text{Y}_8$ alloy in the absence of an interstitial atom. The DOS dip is observed, but is relatively shallow. The lowest position of the DOS is approximately 0.2 eV higher than the E_F . By introducing an Mg, Zn, or Y atom into the center of the cluster, the DOS valley near E_F is more apparent, and the valley width increases compared to the case without an interstitial atom, as shown in Figs. S1(b) – S1(d),. Especially with an interstitial Y atom, the DOS at E_F is reduced, and the width of the DOS valley increases.

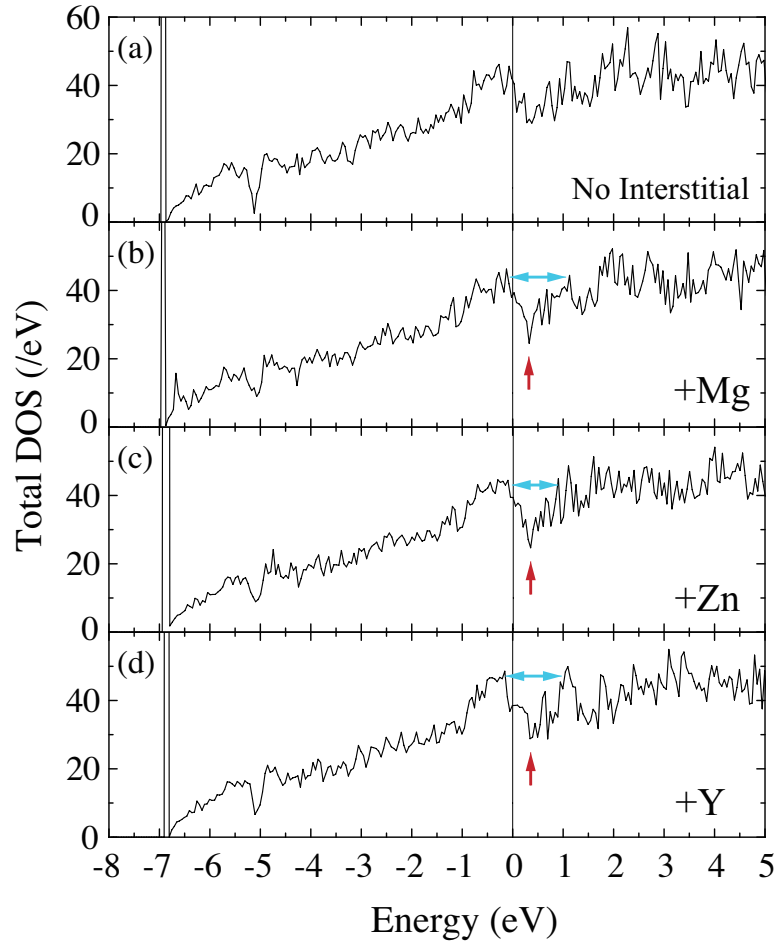


Fig. S1. Total DOS of the 18R-type Mg-Zn-Y alloy (a) without an interstitial atom, and those with an interstitial atom of (b) Mg, (c) Zn, and (d) Y are depicted. The origin in the horizontal axis is taken at the Fermi energy E_F . Double-headed arrows indicate the width of the DOS valley. Up arrows represent the bottom of the DOS valley.

2. Dependence of number of Zn vacancies (x) on total DOS

The dependence of the number of Zn vacancies x on the total DOS is shown in Fig. S2. As x increases from $x = 1$ to $x = 3$ in $\text{Mg}_{58}\text{Zn}_{7-x}\text{Y}_8$, the valley structure of DOS above the E_F becomes shallow, and the valley width increases. The Fermi level shifts to a high energy position close to the bottom of the DOS valley. The tendency of DOS also suggests that $x = 4$ and $x = 5$ are not stable. However, the change in total DOS in the LPSO-type Mg-Zn-Y alloys is not distinct compared to simple metals with LPSO structures in Fe.¹⁰⁾ Thus, we used the projected DOS on the p orbitals of the Zn and Mg atoms and the d orbitals of the Y atom in the main text to clarify the chemical bond between them and the origin of structural stability.

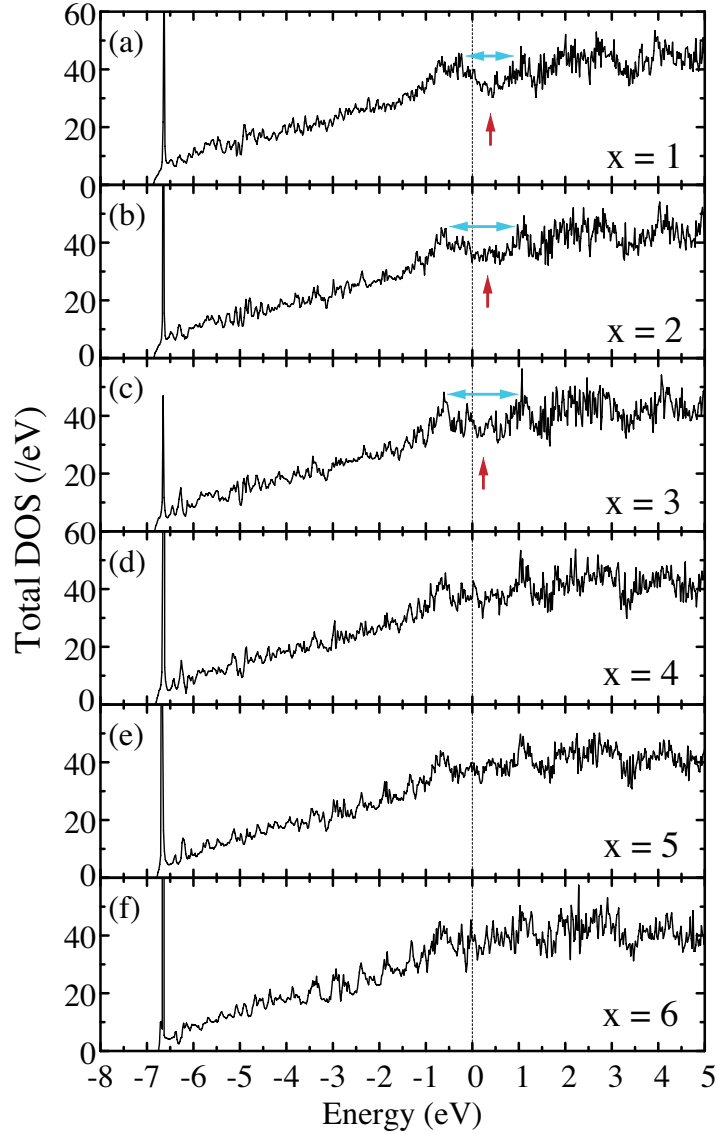


Fig. S2. Total DOS dependent on number of Zn vacancies x in $18R\text{-Mg}_{58}\text{Zn}_{7-x}\text{Y}_8$ alloy: (a) $x = 1$; (b) $x = 2$; (c) $x = 3$; (d) $x = 4$; (e) $x = 5$; (f) $x = 6$. Up arrows represent the bottom of the DOS valley. Double-headed arrows indicate the width of DOS valley.

3. Convex hull diagram

The convex hull plotted in Fig. 2(c) in the main text is obtained with reference energy values at $x = 0$ and $x = 6$. However, the shape of the convex hull may change depending on the choice of reference energy. The formation energy as a function of vacancies x with reference energy values at $x = 0$ and $x = 4$ is calculated as

$$\Delta E(x) = E(\text{Mg}_{58}\text{Zn}_{7-x}\text{Y}_8) - \left\{ \frac{(4-x)}{4} E(\text{Mg}_{58}\text{Zn}_7\text{Y}_8) + \frac{x}{4} E(\text{Mg}_{58}\text{Zn}_3\text{Y}_8) \right\}, \quad (\text{S5})$$

and with reference energy values at $x = 0$ and $x = 5$ is calculated as

$$\Delta E(x) = E(\text{Mg}_{58}\text{Zn}_{7-x}\text{Y}_8) - \left\{ \frac{(5-x)}{5} E(\text{Mg}_{58}\text{Zn}_7\text{Y}_8) + \frac{x}{5} E(\text{Mg}_{58}\text{Zn}_2\text{Y}_8) \right\}. \quad (\text{S6})$$

The convex hulls obtained with the reference energy values at $x = 0$ and $x = 4$, and $x = 0$ and $x = 5$ are plotted in Figs. S3(a) and S3(b), respectively. We came to the same conclusion as we did with $x = 0$ and $x = 6$ as the references.

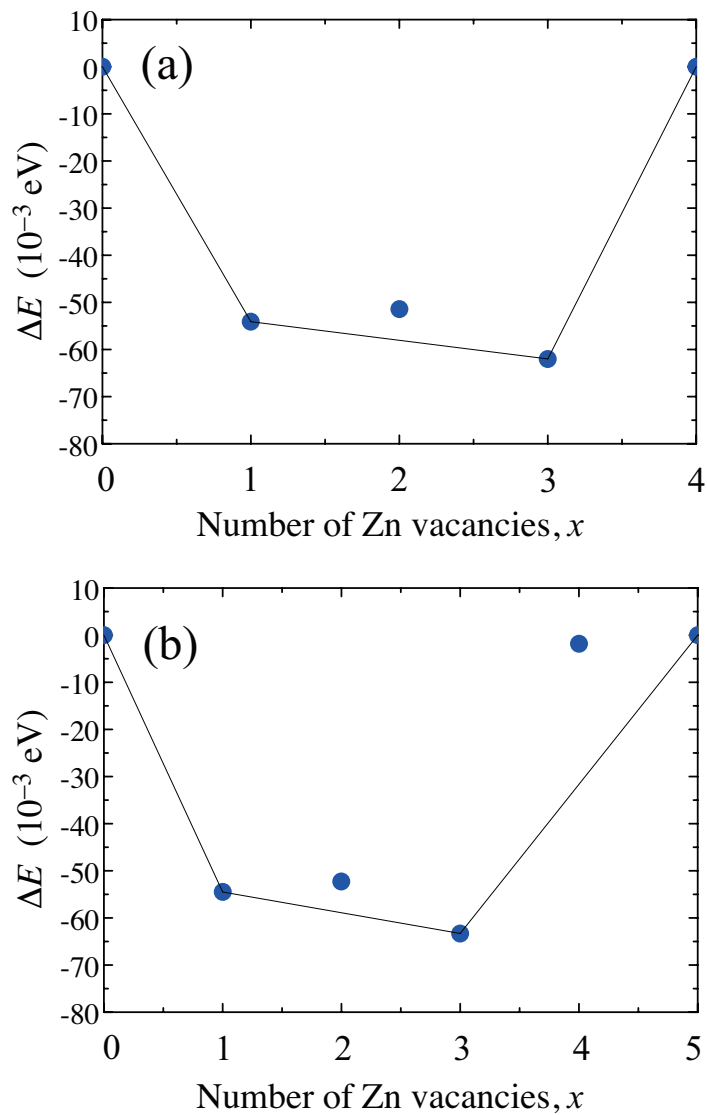


Fig. S3. Convex hull diagrams for number of Zn vacancies (x) in 18R LPSO structure with chemical formula of $\text{Mg}_{58}\text{Zn}_{7-x}\text{Y}_8$, with reference energies are set at (a) $x = 0$ and $x = 4$, and (b) $x = 0$ and $x = 5$. The formation energies are calculated using Eqs. (S5) and (S6), respectively.

4. Details of structural optimizations

4.1 Elemental hcp metal

The lattice parameters of the hcp structure of elemental metals (Mg, Zn, and Y) are also optimized using the first-principles method. The total energies are used as a reference to obtain the heat of formation. The dimensions of the mesh of k points for hcp metals is $20 \times 20 \times 8$. We used the stress tensor for structural relaxations and set the cutoff energies for plane waves and potential as 90 Ry and 588 Ry, respectively. Table S2 presents the DFT-optimized lattice parameters. The hcp Mg shows a nearly ideal c/a ratio. Zn has a c/a ratio greater than the ideal value of $\sqrt{8/3} = 1.633$. In contrast, hcp Y has a smaller c/a ratio than ideal. These results are in agreement with those reported in previous studies.¹¹⁾

Table S2. Optimized structural parameters for hcp structure of elemental metals. The ground states of these metals have an hcp structure with the space group of $P6_3/mmc$. The internal position is $2d$ site at $(1/3, 2/3, 3/4)$.

Element	a [Å]	c [Å]	c/a
Mg	3.19	5.17	1.619
Zn	2.66	4.93	1.854
Y	3.65	5.73	1.572

4.2 18R LPSO structure

To obtain the calculated heats of formation, we performed structural optimization for the lattice parameters and internal atomic coordinates of the Mg-Zn-Y alloys containing Zn vacancies. The convergence threshold for forces for ionic minimization is 0.0001 Ry/Bohr. The calculated total energy has a precision of 0.001 Ry/atom; the difference between different structures (heat of formation) has a higher precision of approximately 0.0001 Ry/atom. We checked the convergence of k -point meshes and the plane-wave cutoffs for the wavefunctions and charge densities. The cutoff energies for plane waves, and charge densities and potential are set at 90 and 588 Ry, respectively. The dimensions of the k -point mesh are $6 \times 6 \times 4$ using the Gaussian smearing method during self-consistent loops, where the width of the smearing function is 0.02 Ry. The convergence threshold for the self-consistent loop is 10^{-8} Ry.

Table S3 presents the distances from the Zn atoms forming the cage composed of Zn and Y atoms to the four closest Mg atoms in the theoretically optimized structures. Their atomic geometries are depicted in Fig. S4. Their atomic coordinates and lattice parameters are presented in Tables S4, S5, and S6, respectively. Of the four bonds between the closest Mg

atoms to the Zn atom, at $x = 1$, the length between Zn2 (Zn3) and Mg15 (Mg16) decreased by 0.01 Å from that at $x = 0$, due to the formation of a Zn vacancy. At $x = 3$, the distances from Zn2 (Zn3) to Mg15 (Mg20) and Mg13 (Mg20) decreased to ~ 2.755 Å, compared to ~ 2.775 Å at $x = 0$. These reductions in bond length suggest a strengthening of the bond between Mg and Zn.

Table S3. Interatomic distances (d) to the four closest Mg atoms from Zn atom forming the Zn_6Y_8 cage in the theoretically optimized structure. The labels of the four nearest Mg atoms in the atomic coordinates are shown in parentheses. The atomic coordinates at $x = 0, 1$, and 3 are presented in Tables S4, S5 and S6, respectively. The labels in square brackets correspond to the labels of atoms in Fig.3 (in the main text).

$x = 0$	Label	Wyckoff position	$d(\text{Zn-Mg})$ [Å]	$d(\text{Zn-Mg})$ [Å]	$d(\text{Zn-Mg})$ [Å]	$d(\text{Zn-Mg})$ [Å]
Fig.3(a)	Zn2	8j	2.776 (Mg8)	2.776 (Mg7)	2.809 (Mg11)	2.810 (Mg13)
	[Zn(2)]		[Mg(1)]	[Mg(2)]	[Mg(3)]	[Mg(4)]
	Zn3	4i	2.774 (Mg10)	2.774 (Mg10)	2.811 (Mg12)	2.811 (Mg12)
$x = 1$	Zn2	4b	2.789 (Mg13)	2.761 (Mg15)	2.810 (Mg25)	2.809 (Mg21)
	Zn3	4b	2.772 (Mg14)	2.766 (Mg16)	2.810 (Mg22)	2.799 (Mg26)
Fig.3(b)	[Zn(2)]		[Mg(1)]	[Mg(2)]	[Mg(3)]	[Mg(4)]
	Zn4	2a	2.781 (Mg19)	2.781 (Mg19)	2.810 (Mg24)	2.810 (Mg24)
$x = 2$	Zn2	1a	2.767 (Mg31)	2.773 (Mg26)	2.809 (Mg43)	2.801 (Mg50)
	Zn3	1a	2.768 (Mg29)	2.773 (Mg27)	2.802 (Mg41)	2.804 (Mg51)
	Zn4	1a	2.751 (Mg28)	2.752 (Mg30)	2.804 (Mg52)	2.802 (Mg42)
	Zn5	1a	2.771 (Mg37)	2.767 (Mg39)	2.803 (Mg47)	2.814 (Mg46)
Fig.3(c)	[Zn(2)]		[Mg(1)]	[Mg(2)]	[Mg(3)]	[Mg(4)]
$x = 3$	Zn2	4b	2.755 (Mg15)	2.754 (Mg13)	2.803 (Mg21)	2.804 (Mg25)
	Zn3	2a	2.754 (Mg20)	2.754 (Mg20)	2.806 (Mg23)	2.806 (Mg23)
Fig.3(d)	[Zn(2)]		[Mg(1)]	[Mg(2)]	[Mg(3)]	[Mg(4)]

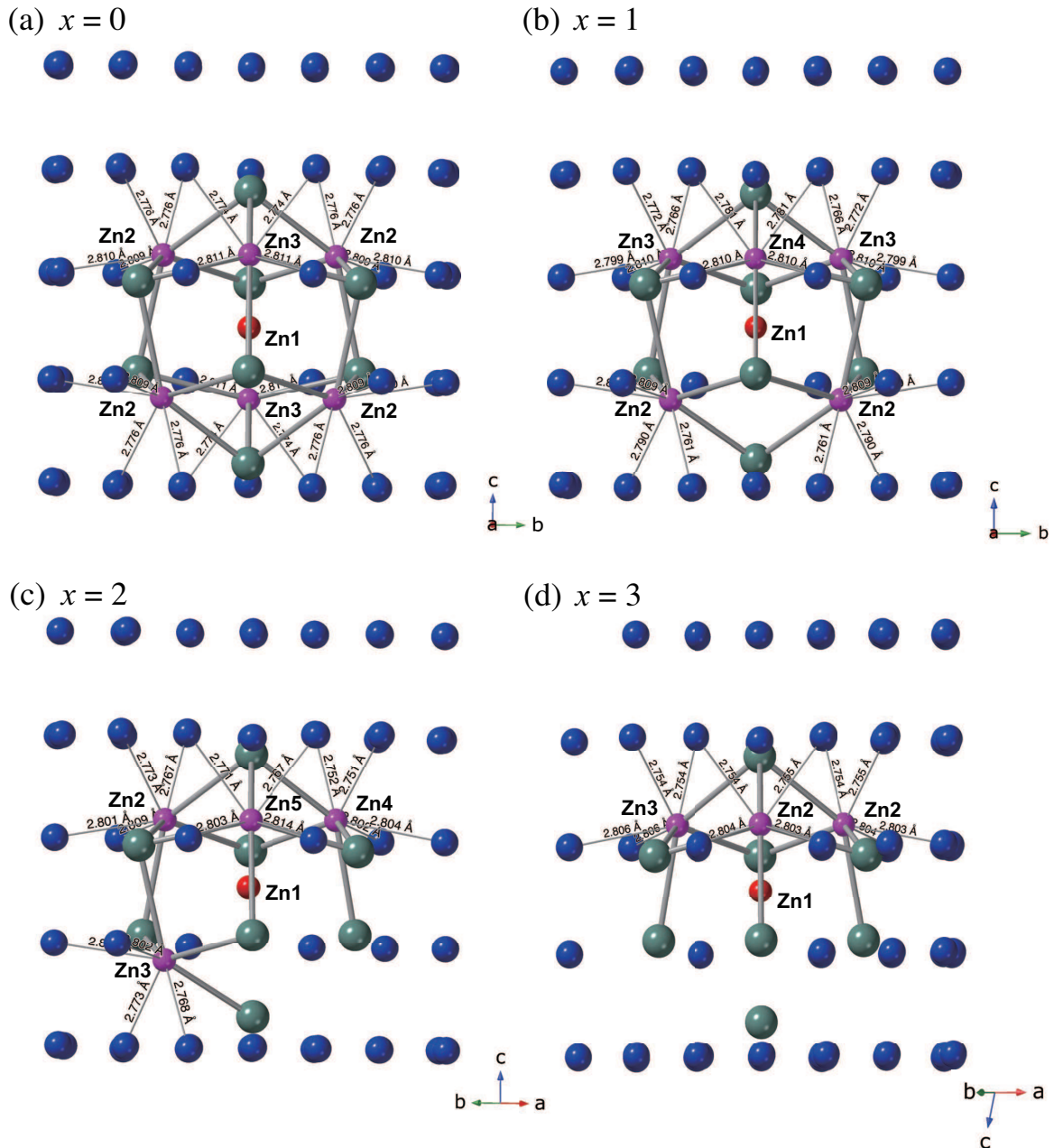


Fig. S4. Atomic structure near the deformed $L1_2$ cluster of solute atoms in $18R \text{Mg}_{58}\text{Zn}_{7-x}\text{Y}_8$ alloy, where (a) $x = 0$, (b) $x = 1$, (c) $x = 2$, and (d) $x = 3$. The distances between Zn and the surrounding Mg atoms are indicated. The blue, purple, and green spheres represent Mg, Zn, and Y, respectively. The c axis in these figures is perpendicular to the basal (0001) plane of the hexagonal lattice.

Table S4. Optimized atomic positions for $18R$ $\text{Mg}_{58}\text{Zn}_7\text{Y}_8$ without Zn vacancy ($x = 0$). The space group is $C2/m$ (No. 12) and the optimized lattice parameters are $a = 11.16$, $b = 19.34$, $c = 16.07 \text{ \AA}$, and $\beta = 103.48^\circ$.

Label	Wyckoff position	fractional coordinates		
		x	y	z
Mg1	$8j$	-0.44129	0.41783	-0.08188
Mg2	$8j$	-0.44602	0.25131	-0.08269
Mg3	$8j$	-0.44458	0.08215	-0.08439
Mg4	$8j$	-0.19317	0.33238	-0.08191
Mg5	$8j$	-0.30518	0.33449	0.08066
Mg6	$8j$	-0.41574	0.33349	-0.24823
Mg7	$8j$	-0.41491	0.16980	-0.24364
Mg8	$8j$	-0.16952	0.41517	-0.24428
Mg9	$8j$	-0.33085	0.25269	0.24884
Mg10	$8j$	-0.34067	0.41496	0.24339
Mg11	$8j$	-0.30906	0.32720	-0.41447
Mg12	$8j$	0.45712	0.41759	-0.41427
Mg13	$8j$	0.43813	0.25530	-0.41430
Mg14	$4i$	0.30910	0	-0.08116
Mg15	$4i$	0.19823	0	0.08487
Mg16	$4i$	0.08925	0	-0.24938
Y1	$8j$	-0.16791	0.35614	0.42821
Y2	$4i$	0.42721	0	0.28123
Y3	$4i$	0.23663	0	-0.42916
Zn1 int	$2d$	0	1/2	1/2
Zn2	$8j$	0.42590	0.11239	-0.38565
Zn3	$4i$	-0.23636	0	-0.38481

Table S5. Optimized atomic positions for $18R \text{Mg}_{58}\text{Zn}_6\text{Y}_8$, where the number of Zn vacancies $x = 1$. The space group is Cm (#8) and the optimized lattice parameters are $a = 11.17$, $b = 19.23$, $c = 16.04 \text{ \AA}$, $\beta = 103.05^\circ$.

Label	Wyckoff position	x	y	z
Mg1	4b	0.44074	0.41757	0.08162
Mg2	4b	0.05906	0.08202	-0.08167
Mg3	4b	0.44451	0.25094	0.08321
Mg4	4b	0.05348	0.24846	-0.08278
Mg5	4b	0.44302	0.08191	0.08499
Mg6	4b	0.05454	0.41778	-0.08460
Mg7	4b	0.19154	0.33272	0.08155
Mg8	4b	0.30621	0.16766	-0.08230
Mg9	4b	0.30474	0.33448	-0.08086
Mg10	4b	0.19320	0.16572	0.08063
Mg11	4b	0.41179	0.33373	0.24755
Mg12	4b	0.08570	0.16665	0.75104
Mg13	4b	0.41134	0.16854	0.24506
Mg14	4b	0.08723	0.32998	0.75670
Mg15	4b	0.16412	0.41580	0.24325
Mg16	4b	0.33169	0.08414	0.75510
Mg17	4b	0.33272	0.25230	0.75066
Mg18	4b	0.16600	0.24676	0.24871
Mg19	4b	0.34313	0.41518	0.75626
Mg20	4b	0.15436	0.08307	0.24557
Mg21	4b	0.30750	0.32543	0.41307
Mg22	4b	0.19353	0.17180	0.58467
Mg23	4b	0.54112	0.41858	0.41159
Mg24	4b	-0.04048	0.08227	0.58493
Mg25	4b	0.56195	0.25608	0.41446
Mg26	4b	-0.05953	0.24454	0.58448
Mg27	2a	0.68999	0	0.07988
Mg28	2a	0.30867	0	-0.08056
Mg29	2a	0.80151	0	-0.08515
Mg30	2a	0.19859	0	0.08819
Mg31	2a	-0.09597	0	0.24742
Mg32	2a	0.09175	0	0.74952
Y1	4b	0.17178	0.35505	0.57232
Y2	4b	0.33416	0.13986	0.42977
Y3	2a	0.57655	0	0.71997
Y4	2a	0.42196	0	0.29026
Y5	2a	0.76610	0	0.42798
Y6	2a	0.24472	0	0.56658
Zn1 int	2a	0.50864	0	0.50393
Zn2	4b	0.57450	0.11223	0.38668
Zn3	4b	-0.07059	0.38746	0.61496
Zn4	2a	0.76500	0	0.61394

Table S6. Optimized atomic positions for $18R \text{Mg}_{58}\text{Zn}_4\text{Y}_8$, where the number of Zn vacancies $x = 3$. The space group is Cm (#8) and the optimized lattice parameters are $a = 11.09$, $b = 19.21$, $c = 16.0 \text{ \AA}$, $\beta = 103.33^\circ$.

Label	Wyckoff position	x	y	z
Mg1	4b	0.44022	0.41795	0.08205
Mg2	4b	0.05644	0.08253	-0.08234
Mg3	4b	0.44654	0.25197	0.08349
Mg4	4b	0.05529	0.24953	-0.08277
Mg5	4b	0.44517	0.08257	0.08337
Mg6	4b	0.05486	0.41816	-0.08815
Mg7	4b	0.19369	0.33221	0.08213
Mg8	4b	0.30716	0.16678	-0.08224
Mg9	4b	0.30594	0.33414	-0.08021
Mg10	4b	0.19482	0.16548	0.08088
Mg11	4b	0.41633	0.33348	0.25022
Mg12	4b	0.08492	0.16639	-0.24629
Mg13	4b	0.41399	0.17034	0.24380
Mg14	4b	0.07991	0.33263	-0.24763
Mg15	4b	0.17082	0.41562	0.24407
Mg16	4b	0.33498	0.08575	-0.24863
Mg17	4b	0.32925	0.25525	-0.24680
Mg18	4b	0.16945	0.24767	0.25156
Mg19	4b	0.33747	0.41846	-0.24800
Mg20	4b	0.15914	0.08563	0.24370
Mg21	4b	0.30985	0.32795	0.41752
Mg22	4b	0.19334	0.17516	-0.41042
Mg23	4b	-0.45473	0.41733	0.41723
Mg24	4b	-0.03922	0.08062	-0.41049
Mg25	4b	-0.43817	0.25479	0.41772
Mg26	4b	-0.06455	0.24427	-0.41014
Mg27	2a	-0.30963	0	0.07941
Mg28	2a	0.30811	0	-0.08105
Mg29	2a	-0.20055	0	-0.08888
Mg30	2a	0.19726	0	0.08438
Mg31	2a	-0.08828	0	0.25163
Mg32	2a	0.09531	0	-0.24764
Y1	4b	0.16069	0.36244	0.43073
Y2	4b	0.33536	0.14204	0.43244
Y3	2a	-0.43404	0	-0.30159
Y4	2a	0.42555	0	0.27588
Y5	2a	-0.23881	0	0.43291
Y6	2a	0.24781	0	-0.43169
Zn1 int	2a	0.49618	0	0.48936
Zn2	4b	-0.42681	0.11199	0.38409
Zn3	2a	0.23739	0	0.38377

References

- 1) D. Egusa, M. Mihalcovic, and E. Abe: Presented at International Symposium on Long-Period Stacking Ordered Structure and Its Related Materials 2012 at Sapporo, October 1-3, 2012.
- 2) J. E. Saal and C. Wolverton: *Scripta Mater.* **67** (2012) 798.
- 3) J. E. Saal and C. Wolverton: *Acta Mater.* **68** (2014) 325.
- 4) K. Kishida, K. Nagai, A. Matsumoto, A. Yasuhara, and H. Inui: *Acta Mater.* **99** (2015) 228.
- 5) M. Itakura, M. Yamaguchi, D. Egusa, and E. Abe: *Acta Mater.* **203** (2021) 116491.
- 6) J. C. Slater: *Quantum Theory of Molecules and Solids II* (McGraw-Hill, 1965).
- 7) S. Inoue and J. Yamashita: *J. Phys. Soc. Jpn* **35** (1973) 677.
- 8) J. Yamashita: *Kotai-densiron (in Japanese)* (Asakura Publishing Co., Ltd., 1973).
- 9) A. T. Paxton, M. Methfessel, and D. G. Pettifor: *Proc. R. Soc. Lond. A* **453** (1997) 1493.
- 10) T. Tsumuraya, I. Watanabe, and T. Sawaguchi: *Phys. Rev. Research* **3** (2021) 033215.
- 11) C. Albrecht, A. Kumar, S. Xu, A. Hunter, and I. J. Beyerlein: *Phys. Rev. Materials* **5** (2021) 043602.